Rydberg-blockade effects in Autler-Townes spectra of ultracold strontium

B. J. DeSalvo,[1,2] J. A. Aman,[1,2] C. Gaul,[3] T. Pohl,[3] S. Yoshida,[4] J. Burgdörfer,[4] K. R. A. Hazzard,[1,2]
F. B. Dunning,[1] and T. C. Killian[1,2,*]

[1]*Department of Physics and Astronomy, Rice University, Houston, Texas 77251, USA*
[2]*Rice Center for Quantum Materials, Rice University, Houston, Texas 77251, USA*
[3]*Max-Planck Institute for the Physics of Complex Systems, 01187 Dresden, Germany*
[4]*Institute for Theoretical Physics, Vienna University of Technology, 1040 Vienna, Austria, EU*

We present a combined experimental and theoretical study of the effects of Rydberg interactions on Autler-Townes spectra of ultracold gases of atomic strontium. Realizing two-photon Rydberg excitation via a long-lived triplet state allows us to probe the regime where Rydberg state decay presents the dominant decoherence mechanism. The effects of Rydberg interactions are observed in shifts, asymmetries, and broadening of the measured atom-loss spectra. The experiment is analyzed within a one-body density-matrix approach, accounting for interaction-induced level shifts and dephasing through nonlinear terms that approximately incorporate correlations due to the Rydberg blockade. This description yields good agreement with our experimental observations for short excitation times. For longer excitation times, the loss spectrum is altered qualitatively, suggesting additional dephasing mechanisms beyond the standard blockade mechanism based on pure van der Waals interactions.

I. INTRODUCTION

Long-range interactions between Rydberg atoms give rise to the Rydberg-blockade effect [1–3], which is of interest for quantum information [4], quantum optics (see, e.g., [5]), dynamics of driven dissipative systems [6–17], and many-body physics with long-range interactions. The latter category includes transitions to ordered phases of Rydberg excitations or atoms [18–23], realization of spin models on optical lattices [24,25], and phenomena in gases such as three-dimensional solitons [26], roton-maxon excitations [22], and super-solid states [22,23,27,28]. Controlling the strength and shape of interactions by mixing a small amount of Rydberg character into atomic ground-state wave functions using off-resonance optical excitation (Rydberg dressing [22,29–32]) figures prominently in most of these proposals.

In spite of recent advances [32], the controlled generation of unitary interactions in large ensembles remains elusive because of the large loss and dephasing rates observed experimentally [31,33]. Much remains to be understood, especially on how complex processes in dense Rydberg gases affect these systems. These processes include plasma formation [33–35], nonadiabatic level crossings at short range [15], and superradiance [36–39]. The correct description of the correlations induced by Rydberg blockade and Rydberg dressing in very dense gases with strong Rydberg excitation is also an active area of study [30,31].

Many of these open questions have been studied via two-photon Rydberg excitation of alkali-metal atoms in a three-level ladder configuration, where different regimes corresponding to coherent population trapping [40,41], electromagnetically induced transparency (EIT) [37,41–43], and Autler-Townes (AT) spectroscopy [44–46] can be accessed by varying the relative intensity of the two excitation lasers.

For alkali-metal atoms this typically involves a long-lived Rydberg state and a much more rapidly decaying intermediate state, which, for example, requires a strongly driven low-lying transition in order to resolve the structure of AT spectra.

A comprehensive theoretical description of such interacting three-level systems in the presence of dissipation and strong correlations remains a challenge. Previous work studied different regimes and succeeded in describing certain aspects of experiments through, e.g., low-intensity expansions [47], classical Monte Carlo simulations [6,48,49], density-matrix cluster expansions in the limit of low densities [40], and quantum trajectory Monte Carlo simulations of small systems [11,48]. An insightful approach to analyze experimental observation is based on the corresponding single-body optical Bloch equations augmented by additional terms describing interaction-induced Rydberg level shifts as well as dephasing of the Rydberg transition [37,38,42,45,46,50]. Depending on the particular setting, such measurements where found to be consistent with either interaction-induced line shifts [38] or pure dephasing [37,42,45,46,50].

While most experimental work has focused on alkali-metal Rydberg gases, alkaline-earth-metal atoms have attracted significant interest recently because of new possibilities offered by their divalent electronic structure. The principal transition of the Rydberg core, which is typically in the visible, can be used to drive autoionizing transitions [51], to image Rydberg atoms or ions [52], and to provide oscillator strength for magic-wavelength optical trapping of Rydberg atoms [53]. Moreover, there is a greater variety of Rydberg-Rydberg interactions available because of the existence of triplet and singlet excited levels [54]. Compared to alkali-metal atoms [22], two-photon excitation to triplet Rydberg levels via a long-lived triplet state, as demonstrated here, can also reduce the decoherence from light scattering for a given Rydberg state coupling and therefore holds promise for Rydberg dressing in such systems.

In this work we present an experimental study of Rydberg-Rydberg atom interactions in cold

*killian@rice.edu

alkaline-earth-metal earth gases excited via long-lived triplet states. We probe such interactions via AT spectroscopy of dense gases through direct measurements of atomic loss. As a unique feature of our experiment, the long lifetime of the intermediate state enables AT spectroscopy for strongly driven Rydberg transitions, i.e., in the regime of a small Rydberg state population similar to EIT experiments in alkali-metal gases. In contrast to previous studies of related alkali-metal systems [37,38,42,45,46,50], our measurements show clear signatures of both level shifts and decoherence induced by the strong Rydberg-Rydberg atom interactions.

Our theoretical analysis is based on an effective one-body description augmented by nonlinear energy shifts and phenomenological dephasing rates that are proportional to the Rydberg density and obtained from a mean-field description accounting for excitation blockade effects [55]. A comparison to the experimental results for short evolution times suggests that the nonlinear shift and dephasing rate are of equal magnitude and consistent with the calculated value of van der Waals interactions [54] and the associated blockade radius. Reference [56] presents an alternative description of interaction effects in strontium AT spectra based on the master equation for the multiparticle density matrix. At long evolution times we observe an additional loss feature on two-photon resonance that cannot be explained by the sole action of van der Waals interactions between the laser-excited Rydberg states and we provide possible explanations in terms of additional dephasing mechanisms. A deeper understanding and ultimately the control of the observed loss will be important, e.g., for future applications of Rydberg dressing in such systems.

II. EXPERIMENTAL METHODS

We perform our experiments on ^{84}Sr atoms confined in an optical dipole trap (ODT) formed by crossed 1064-nm laser beams with waists of 300 μm (65 μm) and 440 μm (38 μm) in the horizontal (vertical) dimension. These beams propagate in the horizontal plane and cross at a 90° angle. A 1-s hold in the ODT results in several million atoms at a temperature of 700 nK. Evaporative cooling for 5 s produces pure condensates of 4×10^5 atoms. For the experiments described here, however, we halt the evaporation before a Bose-Einstein condensate forms and conduct measurements on a sample with temperature $T \approx 150$ nK. The details of cooling and trapping ^{84}Sr are described elsewhere [57,58].

We excite atoms exclusively to the $5s24s\,^3S_1$ Rydberg state (lifetime $\tau_{3S_1} \approx 4\,\mu$s [59]) with two-photon excitation using the narrow $^1S_0 \to {}^3P_1$ transition ($\tau_{3P_1} = 21\,\mu$s) as the intermediate state (Fig. 1). The first transition is driven using 689-nm light from the laser used for intercombination-line laser cooling. The Rabi frequency for this beam Ω_{01} is determined with an accuracy of 15% by measuring the frequency of $^1S_0 \to {}^3P_1$ Rabi oscillations. For these experiments, we use values of $\Omega_{01}/2\pi$ between 26 and 133 kHz and the detuning of the 689-nm laser from resonance ($\Delta_{01}/2\pi$) is between -2 and 2 MHz.

The upper leg of the two-photon transition is strongly driven using 319-nm radiation generated by frequency-doubling light at 638 nm obtained by sum-frequency mixing of the pump and signal beams in an optical parametric oscillator pumped by
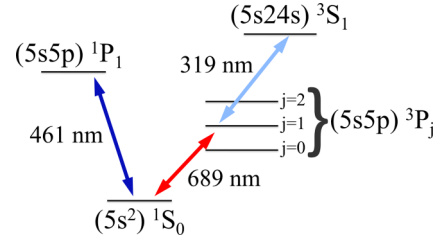

FIG. 1. Partial level diagram for Sr showing all transitions discussed in the text.

a single-frequency fiber laser at 1064 nm. The UV radiation has a full width at half maximum of 300 kHz and is held on resonance with detuning $\Delta_{12} = 0$. The UV light has a beam waist of 600 μm at the atoms and a power of 34 mW, resulting in a Rabi frequency $\Omega_{12}/2\pi = 2.4$ MHz, as determined from the separation of the loss peaks in the AT spectrum (see Fig. 2). The laser beam intensity profiles are much broader than the size of the trapped atom sample ($\sim 45 \times 30 \times 4\,\mu$m^3), so we neglect spatial variation of the Rabi frequencies.

We apply a magnetic field of 1.5 G in the vertical direction, which defines our quantization axis. Electric fields of up to 0.8 V/cm can be applied parallel to the magnetic field using field plates located outside the vacuum viewport windows. The 689-nm light propagates antiparallel to gravity and is circularly polarized to drive the $^1S_0 \to {}^3P_1 (m_j = 1)$ transition. The 319-nm light propagates horizontally and is vertically polarized to drive the $^3P_1(m_j = 1) \to 5s24s\,^3S_1(m_j = 1)$ transition. The timing and power of both lasers are precisely controlled by acousto-optic modulators. The optical dipole trap is left on during excitation and all detunings are measured with respect to line centers that include the ac Stark shift.

After excitation, the atoms are released from the trap and the ground-state atom population is measured with time-of-
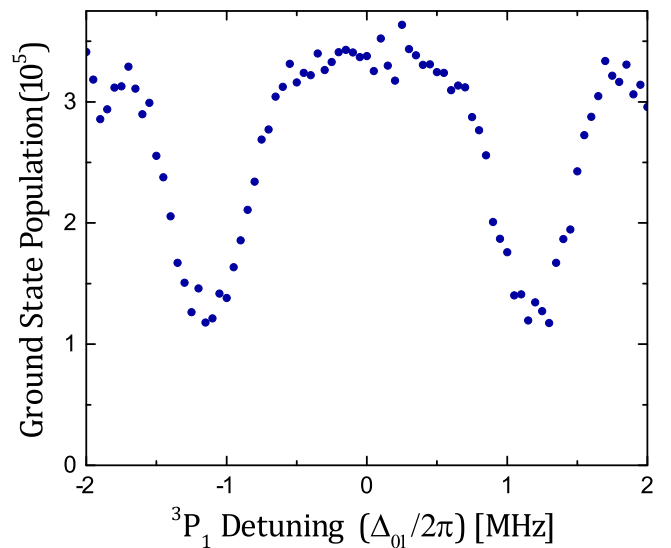

FIG. 2. Autler-Townes spectrum for weak excitation ($\Omega_{01}/2\pi = 26$ kHz) in a low-density ($\rho = 1.9 \times 10^{12}$ cm^{-3}) sample with the 319-nm laser on resonance with the $5s5p\,^3P_1 \to 5s24s\,^3S_1$ transition ($\Delta_{12} = 0$). The loss peaks are spaced by the UV Rabi frequency $\Omega_{12}/2\pi = 2.4$ MHz.
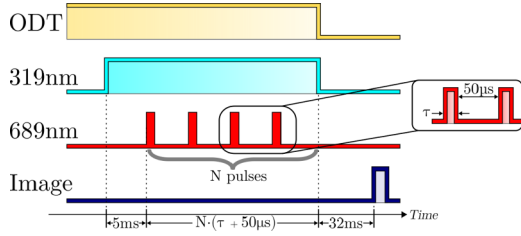
FIG. 3. Timing diagram for recording Autler-Townes spectra. Details are in the text.

flight absorption imaging on the $5s^2\ ^1S_0$–$5s5p\ ^1P_1$ transition at 461 nm. Excitation to the Rydberg level is detected as ground-state atom loss, which can result from direct trap loss through recoil, from decay to the very-long-lived $5s5p\ (^3P_0, ^3P_2)$ states, and through inelastic collisions [60].

For recording loss spectra, we employ the pulsed excitation scheme shown in Fig. 3. We first turn on the 319-nm laser; 5 ms later, we apply a series of N pulses of the 689-nm laser, with N chosen to yield approximately 50% peak loss. After the pulse sequence, the UV light remains on for 50 μs. All light is then extinguished and the atoms are released from the trap and imaged after a 32-ms time of flight.

The 689-nm pulses have a preselected on time followed by 50 μs of off time between each pulse. Since our method of detection is counting remaining ground-state atoms, shot-to-shot atom-number fluctuations and other technical sources of noise make it hard to detect the excitation of a small number of Rydberg atoms in a single pulse. By using N pulses, we amplify the loss to get a better signal-to-noise ratio. Because the off time is chosen to be long compared to the lifetime of both the $^3P_1$ and $5s24s\ ^3S_1$ states, the conditions at the start of each pulse are identical up to a change of the total number of atoms. Thus, to a good approximation, the series of short pulses only amplifies the signal in contrast to simply using a longer pulse, which would modify the physics by increasing the excitation fraction. To compare the data to theory at each data point, we assume an exponential decay of atom number with excitation time to estimate the fractional loss for a single pulse.

For taking time-evolution data, the pulse sequence in Fig. 4 is employed. We first turn on the 319-nm light for 5 ms and then apply a single pulse of 689-nm light. This pulse is then followed by 50 μs of just 319-nm light before both the UV and ODT beams are extinguished and the atoms are allowed to fall for a 32-ms time of flight before being imaged.
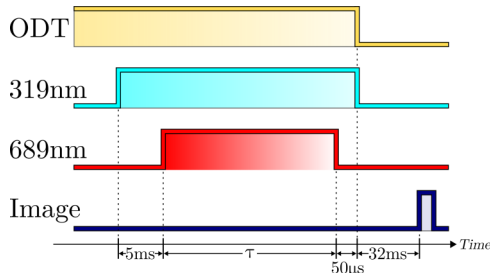

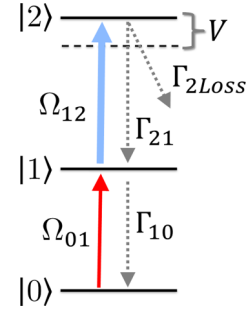FIG. 4. Timing diagram for recording time-evolution data. Details are in the text.

FIG. 5. Simplified level diagram of the three-level system used to model AT spectra.

III. THEORETICAL DESCRIPTION

A. Single-particle density-matrix treatment

In a noninteracting or very-low-density gas, the AT spectrum for the UV laser on resonance consists of two symmetric loss peaks split by the UV Rabi frequency $\Omega_{12}/2\pi$. To model the effects of interactions, we calculate the evolution of the single-particle density matrix σ for a three-level system (Fig. 5) with an approximate treatment of interactions between atoms in the Rydberg state $|2\rangle$ including shifts and a phenomenological dephasing term [39,61]. This approximate treatment is formally similar to a mean-field theory, but includes a simple approximation to the two-body correlations, which are essential to reproduce the scalings found in experiment. The details are discussed in Sec. III B. Spontaneous decay and decoherence can be described using an appropriately chosen Lindblad superoperator $\mathcal{L}(\sigma)$ in the master equation $\dot{\sigma} = \frac{i}{\hbar}[\sigma, H] + \mathcal{L}(\sigma)$. For our system, this results in the optical Bloch equations [39,61]

$$\dot{\sigma}_{00} = \Gamma_{10}\sigma_{11} - \Omega_{01}\,\mathrm{Im}(\sigma_{01}),$$

$$\dot{\sigma}_{11} = -\Gamma_{10}\sigma_{11} + \Gamma_{21}\sigma_{22} + \Omega_{01}\,\mathrm{Im}(\sigma_{01}) - \Omega_{12}\,\mathrm{Im}(\sigma_{12}),$$

$$\dot{\sigma}_{22} = -(\Gamma_{21} + \Gamma_{2\,\mathrm{loss}})\sigma_{22} + \Omega_{12}\,\mathrm{Im}(\sigma_{12}),$$

$$\dot{\sigma}_{01} = -\left(\frac{\Gamma_{10} + \Gamma_{689}}{2} + i\Delta_{01}\right)\sigma_{01} - \frac{i\Omega_{01}}{2}(\sigma_{11} - \sigma_{00})$$
$$+ \frac{i\Omega_{12}}{2}\sigma_{02},$$

$$\dot{\sigma}_{12} = -\left[\frac{\Gamma_{10} + \Gamma_{21} + \Gamma_{2\mathrm{Loss}} + \Gamma_{319} + \Gamma_{\mathrm{Ryd}}\sigma_{22}}{2}\right.$$
$$\left. + i(\Delta_{12} - V_{\mathrm{Ryd}}\sigma_{22})\right]\sigma_{12} - \frac{i\Omega_{12}}{2}(\sigma_{22} - \sigma_{11})$$
$$- \frac{i\Omega_{01}}{2}\sigma_{02},$$

$$\dot{\sigma}_{02} = -\left[\frac{\Gamma_{689} + \Gamma_{21} + \Gamma_{2\mathrm{Loss}} + \Gamma_{319} + \Gamma_{\mathrm{Ryd}}\sigma_{22}}{2}\right.$$
$$\left. + i(\Delta_{01} + \Delta_{12} - V_{\mathrm{Ryd}}\sigma_{22})\right]\sigma_{02} + \frac{i\Omega_{12}}{2}\sigma_{01}$$
$$- \frac{i\Omega_{01}}{2}\sigma_{12},$$

$$(1)$$

where Γ_{ij} denotes the spontaneous decay rate from $|i\rangle \to |j\rangle$, $\Gamma_{2\,\mathrm{loss}}$ denotes spontaneous decay from $|2\rangle$ that results in a
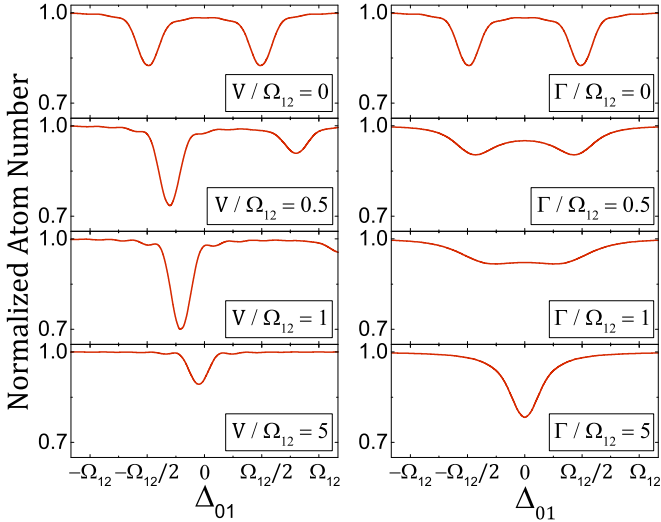
FIG. 6. Calculated effects of a constant level shift V (left) or dephasing Γ (right) on Autler-Townes spectra for $\Delta_{12} = 0$, a single-excitation pulse of duration $t = 2\,\mu$s, and Rabi frequencies $\Omega_{01}/2\pi = 133$ kHz and $\Omega_{12}/2\pi = 2.4$ MHz. The values of V and Γ are as indicated.

loss of atoms such as decay into $5s5p\,^3P_2$ and $5s5p\,^3P_0$ states, and Γ_{689} and Γ_{319} are the dephasing rates due to respective laser linewidths. The Rabi frequencies are time dependent to accommodate nonsimultaneous laser on and off times.

From fitting our low-density and weak-excitation data, we estimate $\Gamma_{689} = 120 \times 10^3$ s^{-1} and $\Gamma_{319} = 1.2 \times 10^6$ s^{-1}. This is consistent with analysis of our laser lock circuitry and other spectral measurements. The decay rate of the $^3P_1$ state is known very accurately. However, the decay rate of the excited state is less well known. We obtain the best agreement with our data using a decay rate of $\Gamma_{21} + \Gamma_{2\,\mathrm{loss}} = 310 \times 10^3$ s^{-1}, which is slightly higher than the natural decay rate expected from scaling the results of [59]. The branching ratio calculated from the Wigner-Eckart theorem would imply that $1/3$ of the decays from the Rydberg state result in $^3P_1$ atoms, but the recoil energy for a single 320-nm photon exceeds the trap depth, so we assume all radiative decay leads to atom loss and set $\Gamma_{21} = 0$. This slightly improves agreement between simulation and data.

In Eq. (1), $V_{\mathrm{Ryd}}\sigma_{22}$ describes the level shift due to interactions (in units of radial frequency) within our approximations and $\Gamma_{\mathrm{Ryd}}\sigma_{22}$ describes a phenomenological dephasing due to Rydberg-Rydberg interactions. The influence of each will depend on the density of Rydberg atoms through the factor σ_{22} and whatever the density dependence is in V_{Ryd} and Γ_{Ryd}, but to understand the effects of these terms we first display AT spectra calculated with $V_{\mathrm{Ryd}}\sigma_{22}$ and $\Gamma_{\mathrm{Ryd}}\sigma_{22}$ replaced with constants V and Γ.

In the left panel of Fig. 6, we see that increasing V leads to a blueshift and an asymmetry in the spectrum, similar to increasing the detuning of the UV laser Δ_{12}. At large V, loss occurs close to two-photon resonance ($\Delta_{01} \approx 0$), but it is strongly suppressed. In our system, loss only occurs from the Rydberg state, and for large Δ_{12} or V, the eigenstate resonantly excited at $\Delta_{01} \approx 0$ has diminishing Rydberg character.

The effect of increased dephasing is markedly different. There is no shift and no asymmetry in the loss features, and at low values of Γ only a reduction of the splitting and a broadening of the peaks are evident. For large values of Γ, a very strong loss feature arises at two-photon resonance, implying a large fraction of Rydberg character in the excited state. This can be understood in the limit of extremely large dephasing, in which the coherence between the intermediate and Rydberg states is never formed. Excitation to the intermediate state results in loss without the appearance of AT splitting. From these plots, it is evident that the effects of V and Γ are largely separable in AT spectra.

B. Theory of Rydberg-Rydberg interactions with two-body correlations arising from blockade

The interaction between two $5s24s\,^3S_1$ Rydberg atoms at an interatomic separation r can be described with an isotropic repulsive van der Waals interaction (in frequency units) $V(r) = C_6/\hbar r^6$, with $C_6/\hbar = 8.8 \times 10^6\ \mu$m^6 s^{-1} [54]. We begin by recalling the mean-field theory, in which the many-body interacting system is replaced by a model of one atom in an external potential determined by the average density of other particles,

$$V_{\mathrm{MF}} = \int d\mathbf{r}'\, V(\mathbf{r}')\langle n_2(\mathbf{r}')\rangle. \tag{2}$$

For a translationally invariant system, the density of Rydberg atoms is taken as a constant $\langle n_2(\mathbf{r}')\rangle = \sigma_{22}\rho$. The mean-field approximation neglects all correlations, which for the present system leads to severe inaccuracies. In particular, one finds that V_{MF} diverges.

This divergence results from a failure to reasonably describe short-range correlations. We expect strong effects from the Rydberg blockade, which prevents excitation of a second Rydberg atom within a blockade radius $R_B = (C_6/2\hbar\Omega_{12})^{1/6}$ of an atom that is already in the Rydberg state. This creates spatial correlations in the positions of excited atoms, which are neglected in a mean-field treatment. We can approximately incorporate correlations into the description by introducing a short-range cutoff to the spatial integral at R_B,

$$V_{\mathrm{eff}} = \int_{R_B}^{\infty} d\mathbf{r}\, \frac{C_6}{\hbar r^6}\langle n_2(\mathbf{r})\rangle = \frac{C_6\sigma_{22}\rho}{\hbar}4\pi \int_{R_B}^{\infty} dr\, r^{-4}$$
$$= \frac{4\pi C_6}{3\hbar R_B^3}\sigma_{22}\rho. \tag{3}$$

This goes beyond mean-field theory by incorporating hard-core pair correlations between the Rydberg states in a manner analogous to Ref. [55]. However, the approximations made are quite drastic: They incorporate only pairwise correlations, correlations are only between the Rydberg levels, and the correlations are imposed with a rather crude hard-core step function. Remarkably, we will see that this approximate description of the Rydberg level shift due to interactions suffices to quantitatively reproduce much of our data. It yields $V_{\mathrm{Ryd}} = 4\pi C_6\rho/3\hbar R_B^3$ in Eq. (1).

Figure 7 shows the typical strength of interactions for various experimental conditions and the predicted C_6 value [54]. In our experiments, $R_B = 0.8\ \mu$m. In this approach,
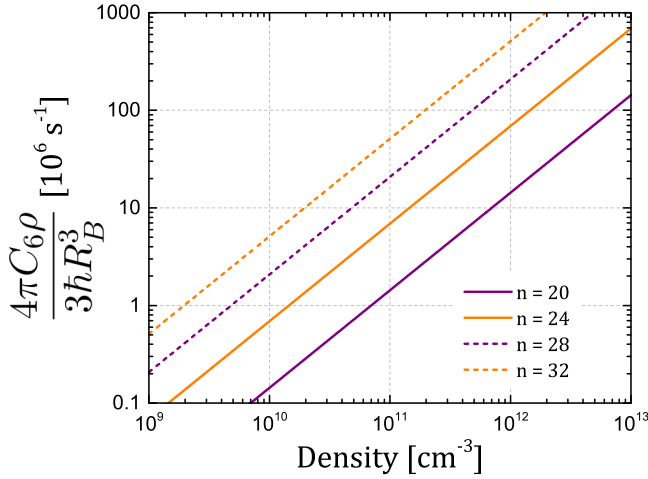
FIG. 7. Interaction energy coefficient $4\pi C_6\rho/3\hbar R_B^3$ predicted from the blockade-corrected mean-field approximation in Eq. (3) as a function of density ρ for $^3S_1$ Rydberg atoms with the indicated principal quantum numbers n and $\Omega_{12}/2\pi = 2.4$ MHz.

we have neglected the effects of level crossings with other molecular potentials, as well as effects due to higher-order terms in the multipole expansion. Both should only be important at internuclear distances less than R_B for our experimental parameters.

A unique feature of this work with strontium is that the linewidth of the intermediate $^3P_1$ state $\Gamma_{10} = \Gamma_{^3P_1} = 47 \times 10^3$ s^{-1} is much smaller than the linewidth of intermediate states used in experiments with alkali-metal atoms. This allows us to be in the AT regime rather than the EIT regime even though we are strongly driving the $^3P_1$-Rydberg transition. If one defines a general blockade radius as $R_B = (C_6/2\hbar\gamma)^{1/6}$, then $\gamma = \Omega_{12}^2/\Gamma_{10}$ in the EIT regime, while $\gamma = \Omega_{12}$ in our experiments.

Starting from the calculation of the level shift including correlation effects, we treat density inhomogeneity in our trapped gas within a local-density approximation (LDA). The observable I (typically the total number of ground-state atoms remaining after a period of excitation in a trap) is calculated theoretically as an integral over density of I evaluated for fixed density $I(\rho)$ with weighting determined by the distribution of densities in the trap,

$$I = \int_0^{\rho_0} I(\rho)g(\rho)d\rho/n, \tag{4}$$

where ρ_0 is the peak density and $g(\rho)$ is the weighting function

$$g(\rho) = \frac{2\pi}{\omega_1\omega_2\omega_3}\left(\frac{2k_BT}{m}\right)^{3/2}\left[\ln\left(\frac{\rho_0}{\rho}\right)\right]^{1/2} \tag{5}$$

for the harmonic trap oscillation frequencies ω_i and total number of trapped atoms n. The length scale for density variation in the trap (given by the density distribution) is long compared to the blockade radius, interatomic spacing, and the distance a Rydberg atom travels in its lifetime, justifying the use of the LDA. We numerically evaluate the integral in Eq. (4) with an 11-point trapezoidal rule approximation.

While the form of V_{Ryd} follows from a physical model of the effects of Rydberg blockade on excitation correlations,

a microscopic picture for interaction-induced dephasing is less obvious. We qualitatively discuss possible sources of this dephasing in Sec. IV. Experimentally, we find that most of our data can be well described assuming the dephasing is similar in magnitude to the level shift. We thus use $\Gamma_{\mathrm{Ryd}} = \beta 4\pi C_6\rho/3\hbar R_B^3$ in Eq. (1) and treat β as an adjustable parameter.

IV. RESULTS AND DISCUSSION

A. Spectra for short excitation times

Short-time dynamics were probed using excitation pulses of 2-μs duration and the timing sequence illustrated in Fig. 3 and described in Sec. II. The UV laser is held on resonance $\Delta_{12} = 0$ and the frequency of the 689 nm laser is scanned to obtain AT spectra. Spectra were recorded for a series of 689-nm laser intensities corresponding to $\Omega_{01}/2\pi = \{26,56,92,133\}$ kHz. Higher Ω_{01} in general corresponds to a higher Rydberg excitation rate. The number of pulses is adjusted for each spectrum to produce peak depletion of the ground state of about 50% at the end of the pulse sequence. However, to facilitate discussion and comparison with simulation, the loss after a single pulse is estimated assuming an exponential decay of atom number at each frequency point. Spectra are presented for two different peak densities $\rho_0 = 1.9 \times 10^{12}$ cm^{-3} (Fig. 8) and $\rho_0 = 1 \times 10^{13}$ cm^{-3} (Fig. 9). For principal quantum number $n = 24$, with $\Omega_{12} = 2.4$ MHz, the blockade density is $\rho_B = (4\pi R_B^3/3)^{-1} = 4.2 \times 10^{11}$ cm^{-3}. Therefore, for the presented peak densities the numbers of atoms within a blockade volume are $\rho_0/\rho_B \sim 5$ and 25. We note that the low- and high-density data are both recorded using the same ODT configuration.

For the low-density data (Fig. 8), the lowest excitation strength (top) results in an almost symmetric spectrum typical of a noninteracting gas. Each loss peak at $\Delta_{01} = \pm\Omega_{12}/2$ represents excitation by the 689-nm laser to one of the dressed states $|^3P_1\rangle \pm |^3S_1\rangle$. The 2-$\mu$s excitation time is comparable to the lifetime of the Rydberg state, so the fraction of atoms lost is close to the relative population of the Rydberg level at the end of the pulse, which peaks at $\sim10^{-2}$. This is supported by the numerical solutions of the optical Bloch equations. At the center of the spectrum ($\Delta_{01} = 0$), vanishingly small loss rates $\sim f\Gamma_{2\,\mathrm{loss}}$ are expected from scattering in the wings of the symmetric peaks [62], where $f = \Omega_{01}^2/\Omega_{02}^2 \sim 1 \times 10^{-4}$ characterizes the fraction of population in the Rydberg state. The data are well described by the noninteracting single-particle density-matrix treatment [Eq. (1)]. The density of Rydberg atoms and the excitation time are small enough that adding interaction terms ($V_{\mathrm{Ryd}} = \alpha 4\pi C_6\rho/3\hbar R_B^3$ and $\Gamma_{\mathrm{Ryd}} = \beta 4\pi C_6\rho/3\hbar R_B^3$ with $\alpha = \beta = 1$) to the optical Bloch equations has no significant effect. We note that all simulations use a value of Ω_{01} 16% higher than determined from independent spectral measurements to get best agreement with the overall intensity of the signal. This is at the upper limit of our uncertainty, but is in reasonable agreement given the simplicity of our theoretical model.

With increasing Ω_{01}, the spectra display a sizable shift and an asymmetry appears in the peak heights, which is a clear indication of effects due to Rydberg-level shifts
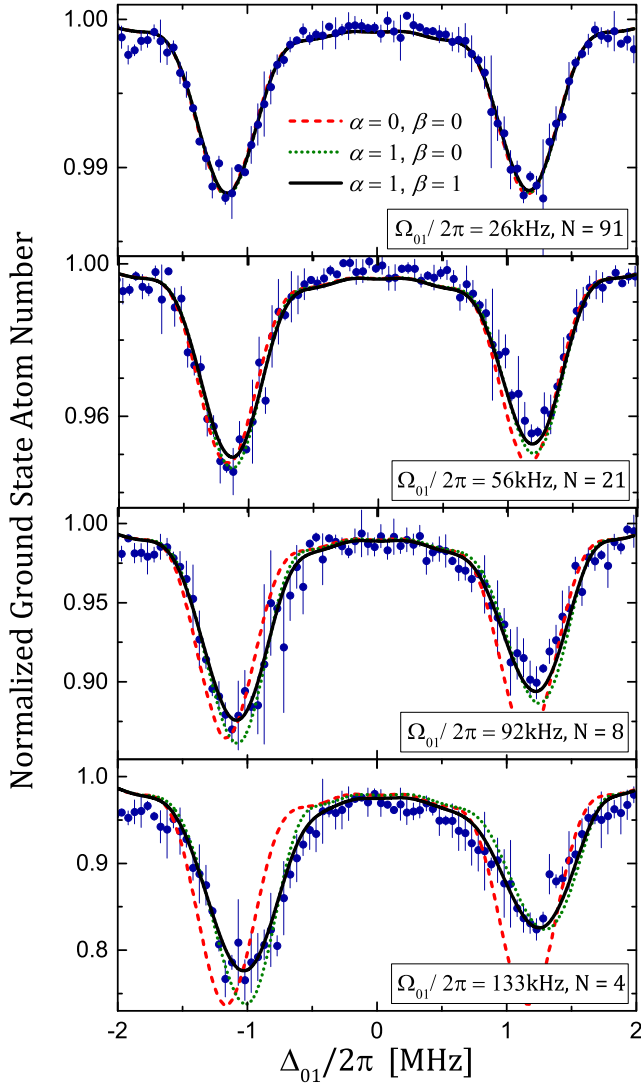
FIG. 8. Blue circles indicate the fractional number of ground-state atoms remaining after a single 2-μs excitation pulse and an initial peak density $\rho_0 = 1.9 \times 10^{12}$ cm^{-3}. The lines show the results of Eq. (1) and the LDA for the interaction terms $V_{\text{Ryd}} = \alpha 4\pi C_6 \rho / 3\hbar R_B^3$ and $\Gamma_{\text{Ryd}} = \beta 4\pi C_6 \rho / 3\hbar R_B^3$, with α and β given in the legend. The simulation is performed for a single 2-μs pulse of 689-nm plus 319-nm excitation, followed by 50 μs of only UV light. The data represent the results of N pulses, but the approximate fraction of atoms remaining after a single pulse is plotted and calculated assuming that the atom number at each frequency point decays exponentially in time; N is indicated in each plot.

induced by Rydberg-Rydberg interactions as described in Fig. 6. These effects are captured very well by adding the blockade-augmented mean-field interaction term V_{Ryd} to the optical Bloch equations. The AT peaks display a pronounced shift to the blue. For a laser detuned slightly to the blue of each unperturbed resonance, this can be interpreted as an antiblockade effect as previously seen in an ultracold Rydberg gas [6,44], in which the interactions shift levels into resonance with the laser.

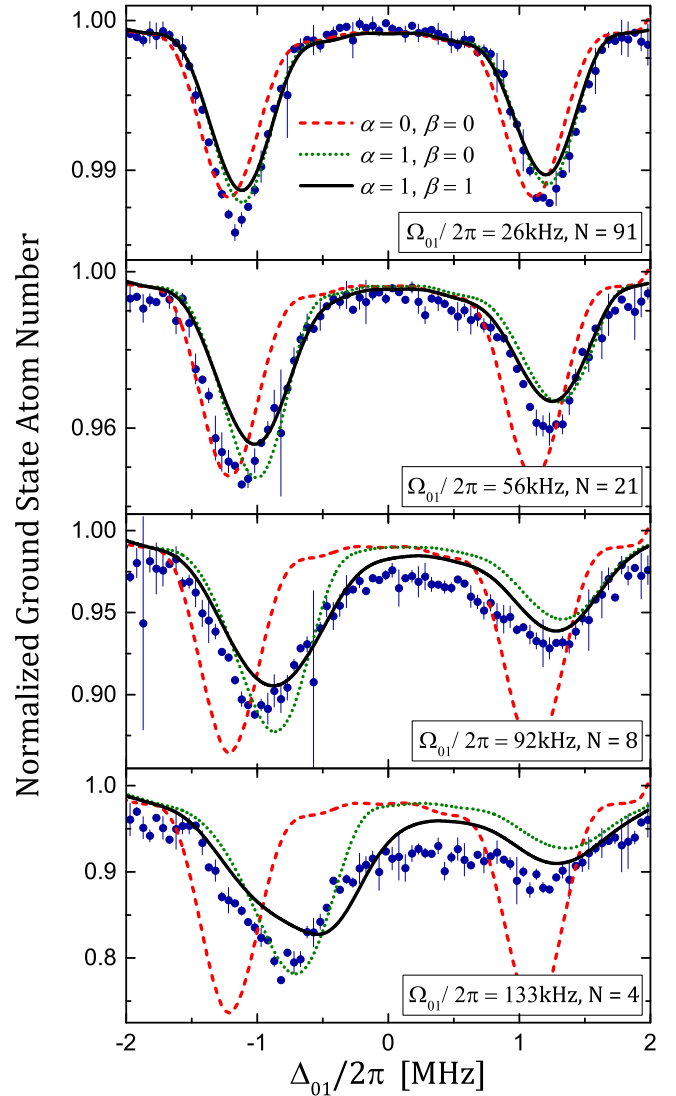Adding interaction-induced dephasing through Γ_{Ryd} with $\beta = 1$ makes a small but noticeable improvement by repro-

FIG. 9. Blue circles indicate the fractional number of ground-state atoms remaining after a single 2-μs excitation pulse and an initial peak density $\rho_0 = 1 \times 10^{13}$ cm^{-3}. Theory lines show the results of Eq. (1) and the LDA for the interaction terms $V_{\text{Ryd}} = \alpha 4\pi C_6 \rho / 3\hbar R_B^3$ and $\Gamma_{\text{Ryd}} = \beta 4\pi C_6 \rho / 3\hbar R_B^3$, with α and β given in the legend. The treatment of the pulse sequences for simulation and data is the same as in Fig. 8.

ducing some of the broadening of the lines. At line center for the highest intensity excitation, the relative population of the Rydberg state is still small, $f = 3 \times 10^{-3}$, and the probability of finding a second excited atom within a blockade radius of a Rydberg atom for peak density $f\rho_0/\rho_{\text{blockade}}$ is $\sim 1 \times 10^{-2}$, so we do not expect Rydberg blockade effects to be important. On resonance with the two AT peaks, however, taking the Rydberg fraction as approximately equal to the loss fraction, we find that $f\rho_0/\rho_{\text{blockade}}$ is on the order of one. This is consistent with the strong interaction effects that are observed.

For the high-density sample (Fig. 9), the spectra show shifts and asymmetries even for the lowest values of Ω_{01}. These spectra are described reasonably well by including the blockade-augmented mean-field interaction term V_{Ryd}, just as in the low-density case. This confirms the linear

scaling with density of the blockade-augmented mean-field level shift, which implies that our modified calculation of the interaction strength incorporating spatial correlations through a short-range cutoff on Rydberg-Rydberg distances [Eq. (3)] captures important aspects of the physics. We conclude that correlations due to the Rydberg blockade effect are playing a strong role during excitation on resonance with the AT peaks in this regime.

The high-density data also display clear signatures of dephasing through the broadening of the lines and increased atom loss at line center. The inclusion of Γ_{Ryd} with $\beta = 1$ improves the agreement, even for very strong interactions ($\Omega_{01}/2\pi = 92$ and 133 kHz). For this level of modification of the spectrum, the dephasing rate Γ_{Ryd} must be interpreted as a phenomenological parameter. A microscopic description of such dephasing terms can be obtained from a more detailed calculation of two-body correlations [41], which goes beyond the scope of the present study.

There is a noticeable discrepancy near the center of the spectrum ($\Delta_{01} = 0$), however, where the experimental data show much more loss than predicted by the simulation, suggesting stronger dephasing rates. To explore this effect, we recorded data with longer excitation times.

B. Spectra for longer excitation times

The short excitation time allows us to observe strong Rydberg interactions, but in a regime in which level shifts are still the dominant effect. At longer excitation times, however, dephasing dramatically alters the excitation dynamics. To probe dynamics on a longer time scale, we obtained AT spectra at high peak density (1×10^{13} cm^{-3}) and high 689-nm intensity ($\Omega_{01}/2\pi = 133$ kHz) for a series of increasing excitation-pulse durations ranging from 2 to 7 μs (Fig. 10). Multiple pulses are applied, following the timing sequence described in Fig. 3. As before, the number of pulses is adjusted for each spectrum to produce peak atom loss of about 50% at the end of the pulse sequence, and for display in the figure and comparison to theory, the spectra are normalized to show the fraction of atoms remaining after a single excitation pulse assuming exponential decay of atom number.

Dephasing corresponding to $\beta = 1$ matches the data for 2-μs excitation time for detuning well removed from the center of the spectrum, while increased dephasing ($\beta = 2$) is required to reproduce the loss near $\Delta_{01} = 0$. The atom-loss spectrum changes dramatically at later times, collapsing to a single peak at line center. This total loss of coherence of the dressed states underlying the AT structure implies dephasing that is much greater than the coupling Rabi frequency Ω_{12} and much greater than the phenomenological dephasing rates that reproduced the short-time spectra. We cannot make a definite statement regarding the form and origin of the dephasing term that might be required to describe this data. However, it is clear that decoherence of the Rydberg level is playing an important role, especially for longer excitation times.

C. Time evolution

The increase in dephasing rate with time can be seen more clearly by directly measuring the time evolution of atom
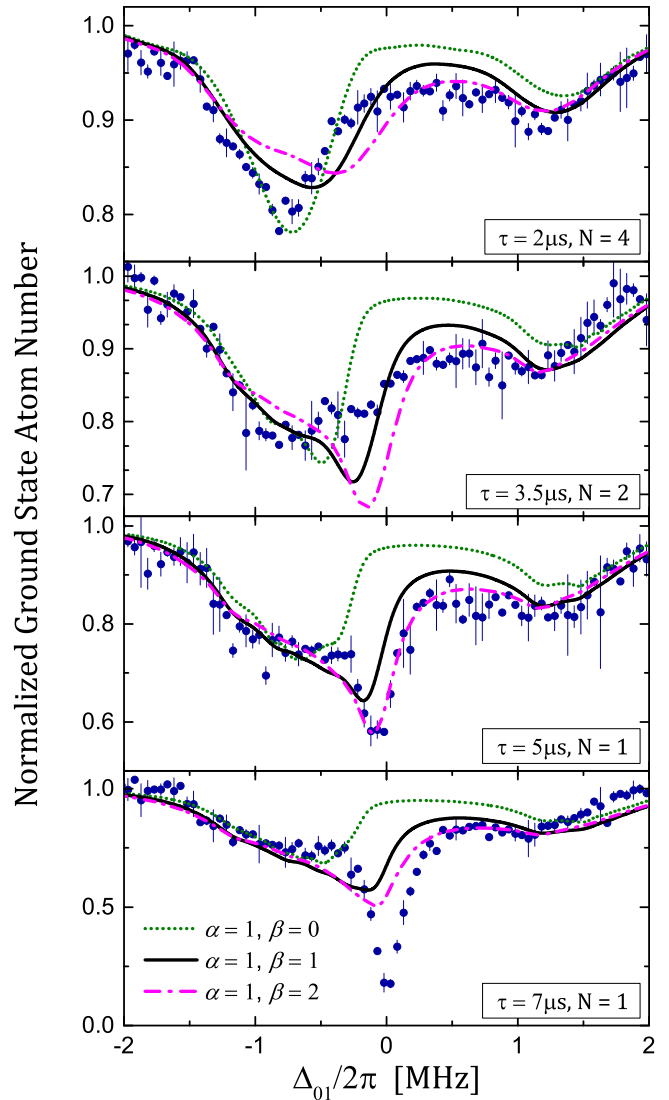

FIG. 10. Blue circles indicate the fractional number of ground-state atoms remaining after a single pulse of length indicated in each plot. The initial peak density is $\rho_0 = 1 \times 10^{13}$ cm^{-3} and $\Omega_{01} = 133$ kHz. (More details are provided in the text.) The lines show the results of Eq. (1) and the LDA for the interaction terms $V_{\mathrm{Ryd}} = \alpha 4\pi C_6 \rho / 3\hbar R_B^3$ and $\Gamma_{\mathrm{Ryd}} = \beta 4\pi C_6 \rho / 3\hbar R_B^3$, with α and β given in the legend. The treatment of the pulse sequences for simulation and data is the same as in Fig. 8.

loss with greater temporal resolution and longer exposure times for high density (1×10^{13} cm^{-3}) and 689-nm laser intensities corresponding to $\Omega_{01}/2\pi = \{20, 40, 90, 133\}$ kHz (Fig. 11). These measurements were performed at the center of the spectrum (Fig. 11, middle) and on resonance with the red-detuned (Fig. 11, left) and blue-detuned (Fig. 11, right) AT peaks observed in the 2-μs spectra.

With $\beta = 1$, we obtain good agreement between the data and model at early times for all experimental conditions. This agreement extends to longer times for detunings on the AT peaks. It is important to note that at different laser excitation frequencies the relative populations of Rydberg and low-lying states are very different, which might result in different dynamics and dominant effects. Near the center of
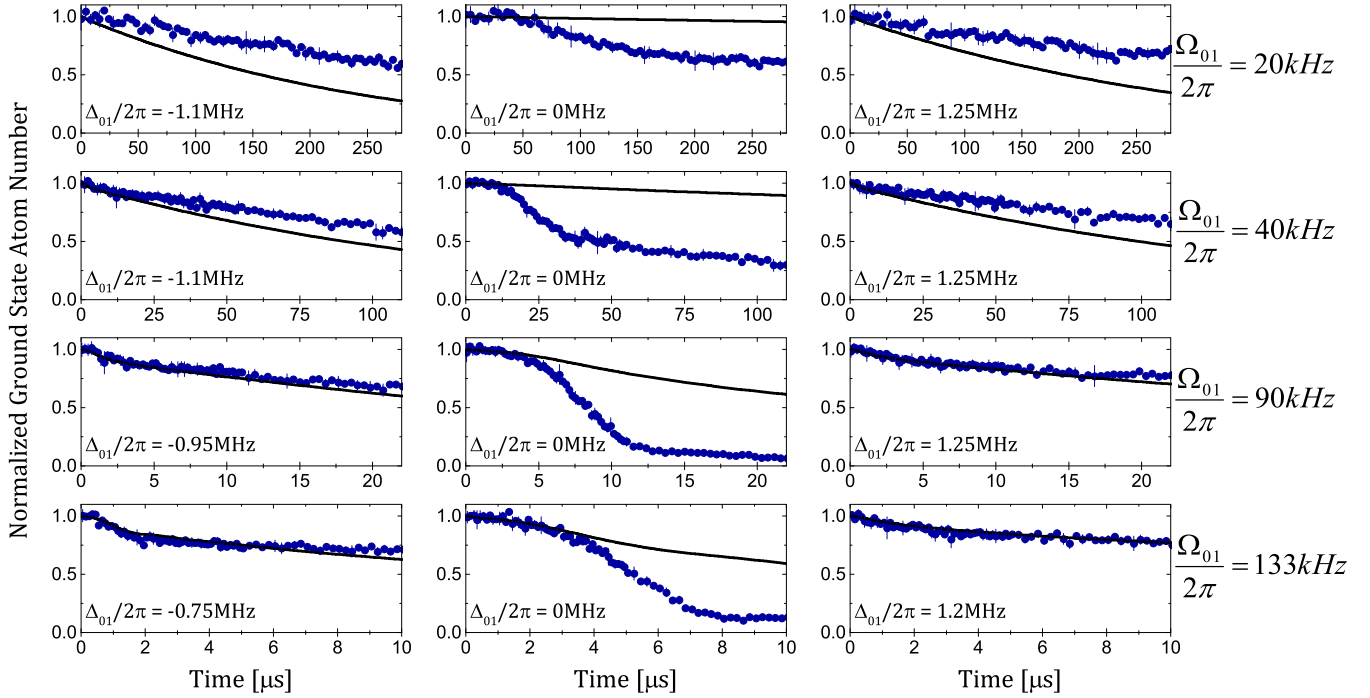
FIG. 11. Fractional number of atoms remaining versus laser excitation time for the 689-laser tuned to the red-detuned (left) and blue-detuned (right) AT peaks and for $\Delta_{01} = 0$ (middle). The initial peak density is $\rho_0 = 1 \times 10^{13}$ cm^{-3}. Detunings of the 689-nm laser are indicated in each figure. Blue circles are experimental data. The lines show the results of Eq. (1) for $V_{\mathrm{Ryd}} = \Gamma_{\mathrm{Ryd}} = 4\pi C_6 \rho / 3\hbar R_B^3$.

the spectrum at $\Delta_{01} = 0$ we observe that theory substantially underestimates the loss at later times. In fact, it appears that the system is well described by moderate dephasing for a short time, which is longer for weaker excitation. Then the system shifts to a different behavior characterized by dramatically increased dephasing. After the overall density of atoms drops below some threshold value, which is lower for stronger excitation, the system appears to revert to the behavior characterized by less dephasing and atom loss. For example, this latter transition occurs after 35 μs of excitation for $\Omega_{01}/2\pi = 40$ kHz.

D. Possible explanations for the increased dephasing

The search for a definitive explanation for the large observed dephasing will be a topic of a future study, but we mention a few possibilities here. The general feature of a delayed turn-on of a very large dephasing rate is consistent with the effects of superradiance [37] out of the $5s24s\,^3S_1$ Rydberg state and/or dipole-dipole interactions [63] between $5s24s\,^3S_1$ atoms and atoms in nearby Rydberg P states populated by natural decay and blackbody radiation.

Other possible sources of dephasing are dc Stark shifts and inelastic collision processes due to free charges present in the excitation volume. Free charges could arise from photoionization of Rydberg atoms, collisions of Rydberg atoms with hot background gas atoms, blackbody radiation, or Penning ionization [35]. The dc Stark shift for the $5s24s\,^3S_1$ Rydberg state is to the red, which would also shift the AT spectrum to the red as a function of Δ_{01}. This is inconsistent with the general blueshift that is observed.

It is beyond the scope of this paper to model collisional processes involving charged particles, but we looked for their influence by testing the effect of an electric field of 0.8 V/cm on the time evolution of trap loss at a fixed detuning of $\Delta_{01} = 0$ and $\Omega_{01} = 40$ kHz. For this field, an ion escapes from the trap on a time scale of 0.1 μs, which is much faster than the atom-loss time scale of tens of μs. If charged particles were important for the dynamics, the dephasing would be much
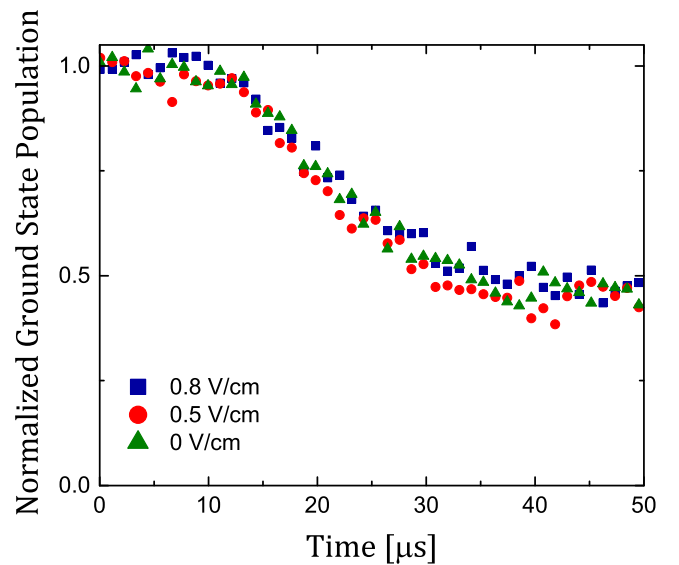

FIG. 12. Time evolution of atom loss at $\Delta_{01} = 0$, $\Omega_{01}/2\pi = 40$ kHz, peak density $\rho_0 = 1 \times 10^{13}$ cm^{-3}, and the indicated applied electric fields.

smaller in the presence of a clearing field. As can be seen from the data plotted in Fig. 12, however, the presence of an applied electric field yielded no effect on the data. This strongly suggests that charged particles are not the cause of the observed dephasing.

V. CONCLUSION

We have presented an experimental study, supported by theoretical modeling, of the effects of Rydberg-Rydberg interactions on the AT spectrum in an ultracold gas of strontium atoms. Results show clearly distinguishable effects associated with shifts and dephasing of the Rydberg level that increase with density and with the Rydberg excitation fraction. We also present an effective potential for the Rydberg level that augments mean-field theory to incorporate the effects of short-range spatial correlations arising from the Rydberg-blockade. With this potential, the density dependence and excitation-strength dependence of loss spectra at short excitation times can be explained with a density-matrix treatment. The local-

density approximation is used to treat the density inhomogeneity of the trapped atom sample. At longer excitation times, the dephasing of the Rydberg level increases dramatically, especially for excitation directly on two-photon resonance $\Delta_{01} = \Delta_{12} = 0$. We suggest superradiance or dipole-dipole interactions as possible explanations for the large dephasing rates.

[1] A. Gaëtan, Y. Miroshnychenko, T. Wilk, A. Chotia, M. Viteau, D. Comparat, P. Pillet, A. Browaeys, and P. Grangier, Nat. Phys. **5**, 115 (2009).

[2] E. Urban, T. A. Johnson, T. Henage, L. Isenhower, D. D. Yavuz, T. G. Walker, and M. Saffman, Nat. Phys. **5**, 110 (2009).

[3] D. Comparat and P. Pillet, J. Opt. Soc. Am. B **27**, A208 (2010).

[4] M. Saffman, T. Walker, and K. Mølmer, Rev. Mod. Phys. **82**, 2313 (2010).

[5] T. Peyronel, O. Firstenberg, Q.-Y. Liang, S. Hofferberth, A. V. Gorshkov, T. Pohl, M. D. Lukin, and V. Vuletić, Nature (London) **488**, 57 (2012).

[6] C. Ates, T. Pohl, T. Pattard, and J. M. Rost, Phys. Rev. A **76**, 013413 (2007).

[7] C. Ates, T. Pohl, T. Pattard, and J. M. Rost, Phys. Rev. Lett. **98**, 023002 (2007).

[8] C. Ates, S. Sevinçli, and T. Pohl, Phys. Rev. A **83**, 041802 (2011).

[9] I. Lesanovsky, Phys. Rev. Lett. **106**, 025301 (2011).

[10] T. E. Lee, H. Häffner, and M. C. Cross, Phys. Rev. Lett. **108**, 023602 (2012).

[11] M. Höning, D. Muth, D. Petrosyan, and M. Fleischhauer, Phys. Rev. A **87**, 023401 (2013).

[12] H. Schempp, G. Günter, M. Robert-De-Saint-Vincent, C. S. Hofmann, D. Breyel, A. Komnik, D. W. Schönleber, M. Gärttner, J. Evers, S. Whitlock *et al.*, Phys. Rev. Lett. **112**, 013002 (2014).

[13] N. Malossi, M. M. Valado, S. Scotto, P. Huillery, P. Pillet, D. Ciampini, E. Arimondo, and O. Morsch, Phys. Rev. Lett. **113**, 023006 (2014).

[14] M. Hoening, W. Abdussalam, M. Fleischhauer, and T. Pohl, Phys. Rev. A **90**, 021603 (2014).

[15] A. Urvoy, F. Ripka, I. Lesanovsky, D. Booth, J. P. Shaffer, T. Pfau, and R. Löw, Phys. Rev. Lett. **114**, 203002 (2015).

[16] I. Lesanovsky and J. P. Garrahan, Phys. Rev. A **90**, 011603 (2014).

[17] H. Schempp, G. Günter, S. Wüster, M. Weidemüller, and S. Whitlock, Phys. Rev. Lett. **115**, 093002 (2015).

[18] T. Pohl, E. Demler, and M. D. Lukin, Phys. Rev. Lett. **104**, 043002 (2010).

[19] R. M. W. van Bijnen, S. Smit, K. A. H. van Leeuwen, E. J. D. Vredenbregt, and S. J. J. M. F. Kokkelmans, J. Phys. B **44**, 184008 (2011).

[20] P. Schauß, M. Cheneau, M. Endres, T. Fukuhara, S. Hild, A. Omran, T. Pohl, C. Gross, S. Kuhr, and I. Bloch, Nature (London) **491**, 87 (2012).

[21] P. Schauß, J. Zeiher, T. Fukuhara, S. Hild, M. Cheneau, T. Macri, T. Pohl, I. Bloch, and C. Gross, Science **347**, 1455 (2015).

[22] N. Henkel, R. Nath, and T. Pohl, Phys. Rev. Lett. **104**, 195302 (2010).

[23] G. Pupillo, A. Micheli, M. Boninsegni, I. Lesanovsky, and P. Zoller, Phys. Rev. Lett. **104**, 223002 (2010).

[24] A. W. Glaetzle, M. Dalmonte, R. Nath, C. Gross, I. Bloch, and P. Zoller, Phys. Rev. Lett. **114**, 173002 (2015).

[25] R. M. W. van Bijnen and T. Pohl, Phys. Rev. Lett. **114**, 243002 (2015).

[26] F. Maucher, N. Henkel, M. Saffman, W. Królikowski, S. Skupin, and T. Pohl, Phys. Rev. Lett. **106**, 170401 (2011).

[27] F. Cinti, P. Jain, M. Boninsegni, A. Micheli, P. Zoller, and G. Pupillo, Phys. Rev. Lett. **105**, 135301 (2010).

[28] M. Boninsegni and N. Prokof'ev, Rev. Mod. Phys. **84**, 759 (2012).

[29] J. Honer, H. Weimer, T. Pfau, and H. P. Büchler, Phys. Rev. Lett. **105**, 160404 (2010).

[30] J. E. Johnson and S. L. Rolston, Phys. Rev. A **82**, 033412 (2010).

[31] J. B. Balewski, A. T. Krupp, A. Gaj, S. Hofferberth, R. Löw, and T. Pfau, New J. Phys. **16**, 063012 (2014).

[32] Y.-Y. Jau, A. M. Hankin, T. Keating, I. H. Deutsch, and G. W. Biedermann, Nat. Phys. **12**, 71 (2016).

[33] T. M. Weber, T. Niederprüm, T. Manthey, P. Langer, V. Guarrera, G. Barontini, and H. Ott, Phys. Rev. A **86**, 020702(R) (2012).

[34] M. P. Robinson, B. Laburthe Tolra, M. W. Noel, T. F. Gallagher, and P. Pillet, Phys. Rev. Lett. **85**, 4466 (2000).

[35] T. C. Killian, T. Pattard, T. Pohl, and J. M. Rost, Phys. Rep. **449**, 77 (2007).

[36] T. Wang, S. F. Yelin, R. Côté, E. E. Eyler, S. M. Farooqi, P. L. Gould, M. Koštrun, D. Tong, and D. Vrinceanu, Phys. Rev. A **75**, 033802 (2007).

[37] K. J. Weatherill, J. D. Pritchard, R. P. Abel, M. G. Bason, A. K. Mohapatra, and C. S. Adams, J. Phys. B **41**, 201002 (2008).

[38] C. Carr, R. Ritter, C. G. Wade, C. S. Adams, and K. J. Weatherill, Phys. Rev. Lett. **111**, 113901 (2013).

[39] F. Karlewski, M. Mack, J. Grimmel, N. Sándor, and J. Fortágh, Phys. Rev. A **91**, 043422 (2015).

[40] H. Schempp, G. Günter, C. S. Hofmann, C. Giese, S. D. Saliba, B. D. DePaola, T. Amthor, M. Weidemüller, S. Sevinçli, and T. Pohl, Phys. Rev. Lett. **104**, 173602 (2010).

[41] S. Sevinçli, C. Ates, T. Pohl, H. Schempp, C. S. Hofmann, G. Günter, T. Amthor, M. Weidemüller, J. D. Pritchard, D. Maxwell *et al.*, J. Phys. B **44**, 184018 (2011).

[42] U. Raitzsch, R. Heidemann, H. Weimer, B. Butscher, P. Kollmann, R. Löw, H. P. Büchler, and T. Pfau, New J. Phys. **11**, 055014 (2009).

[43] J. D. Pritchard, D. Maxwell, A. Gauguet, K. J. Weatherill, M. P. A. Jones, and C. S. Adams, Phys. Rev. Lett. **105**, 193603 (2010).

[44] T. Amthor, C. Giese, C. S. Hofmann, and M. Weidemüller, Phys. Rev. Lett. **104**, 013001 (2010).

[45] H. Zhang, L. Wang, J. Chen, S. Bao, L. Zhang, J. Zhao, and S. Jia, Phys. Rev. A **87**, 033835 (2013).

[46] H. Zhang, L. Zhang, L. Wang, S. Bao, J. Zhao, S. Jia, and G. Raithel, Phys. Rev. A **90**, 043849 (2014).

[47] S. Sevinçli, N. Henkel, C. Ates, and T. Pohl, Phys. Rev. Lett. **107**, 153001 (2011).

[48] M. Gärttner, S. Whitlock, D. W. Schönleber, and J. Evers, Phys. Rev. A **89**, 063407 (2014).

[49] D. W. Schönleber, M. Gärttner, and J. Evers, Phys. Rev. A **89**, 033421 (2014).

[50] T. Baluktsian, B. Huber, R. Löw, and T. Pfau, Phys. Rev. Lett. **110**, 123001 (2013).

[51] J. Millen, G. Lochead, and M. P. A. Jones, Phys. Rev. Lett. **105**, 213004 (2010).

[52] P. McQuillen, X. Zhang, T. Strickler, F. B. Dunning, and T. C. Killian, Phys. Rev. A **87**, 013407 (2013).

[53] R. Mukherjee, J. Millen, R. Nath, M. P. A. Jones, and T. Pohl, J. Phys. B **44**, 184010 (2011).

[54] C. L. Vaillant, M. P. A. Jones, and R. M. Potvliege, J. Phys. B **45**, 135004 (2012).

[55] H. Weimer, R. Löw, T. Pfau, and H. P. Büchler, Phys. Rev. Lett. **101**, 250601 (2008).

[56] C. Gaul, B. J. DeSalvo, J. A. Aman, F. B. Dunning, T. C. Killian, and T. Pohl, arXiv:1511.06424.

[57] Y. N. Martinez de Escobar, P. G. Mickelson, M. Yan, B. J. DeSalvo, S. B. Nagel, and T. C. Killian, Phys. Rev. Lett. **103**, 200402 (2009).

[58] B. J. DeSalvo, Ph.D. thesis, Rice University, 2015.

[59] S. Kunze, R. Hohmann, H.-J. Kluge, J. Lantzsch, L. Monz, J. Stenner, K. Stratmann, K. Wendt, and K. Zimmer, Z. Phys. D **27**, 111 (1993).

[60] B. J. DeSalvo, J. A. Aman, F. B. Dunning, T. C. Killian, H. R. Sadeghpour, S. Yoshida, and J. Burgdörfer, Phys. Rev. A **92**, 031403 (2015).

[61] M. Tanasittikosol, C. Carr, C. S. Adams, and K. J. Weatherill, Phys. Rev. A **85**, 033830 (2012).

[62] P. M. Anisimov, J. P. Dowling, and B. C. Sanders, Phys. Rev. Lett. **107**, 163604 (2011).

[63] W. R. Anderson, J. R. Veale, and T. F. Gallagher, Phys. Rev. Lett. **80**, 249 (1998).